Review of Scientific Instruments

Design and construction of a new steady-state apparatus for medium thermal conductivity measurement at high temperature

Cite as: Rev. Sci. Instrum. **88**, 104903 (2017); https://doi.org/10.1063/1.5006529
Submitted: 19 October 2016 • Accepted: 25 September 2017 • Published Online: 12 October 2017

Yong Wang, Peng Xiao and Jingmin Dai

Design and construction of a new steady-state apparatus for medium thermal conductivity measurement at high temperature

Yong Wang, Peng Xiao, and Jingmin Dai[a)]
School of Electrical Engineering and Automation, Harbin Institute of Technology, Harbin 150001, China

(Received 19 October 2016; accepted 25 September 2017; published online 12 October 2017)

A new steady-state apparatus is designed and constructed for the measurement of thermal conductivity (up to 25 W/mK) on a square specimen (300 mm side) with a heating temperature range from 30 °C to 900 °C. A vacuum container, of which the pressure can reach to 1 Pa, is also built for materials which can be easily oxidized. The structure of the facility is different from that of traditional steady-state devices, especially for the design of heating plate and heat sink. To verify the temperature uniformity of the heating plate, a simulation analysis is carried out in this paper. Besides, the heating system, the heat sink, the measuring system, and the vacuum system are presented in detail. In addition, the thermal conductivities of a heat insulation tile, 304L stainless steel, *n*-docosane, and erythritol are measured by this apparatus. Finally, an uncertainty analysis is discussed depending on different temperatures and materials. *Published by AIP Publishing.*
https://doi.org/10.1063/1.5006529

I. INTRODUCTION

Thermal conductivity is a significant parameter which cannot be ignored in thermal properties, especially for metal material, thermal insulation material, or phase change material. The steady-state method is generally recognized as the primary method to measure thermal conductivity directly. It is well known that this method is established by a uniform stationary heat flow across the specimen. Furthermore, it is a useful method for measuring thermal conductivity of a large sample.

In recent years, thermal conductivity instruments based on the steady-state method with only one specimen had been designed, constructed, and improved by numbers of scientists. Most of them developed apparatuses based on the traditional guarded hot plate (GHP) method operating from −195 to 800 °C for the measurement of medium thermal-conductivity materials (up to 5 W/mK).[1–4] The similarity of their devices is that the heat flow is obtained from the power of the heater, where the power is measured by the voltage and the corresponding current. In addition, other scientists designed devices by using the heat flux sensor to expand the measurement upper limit to 10 W/mK with the expanded uncertainty (k = 2) of ±6%.[5,6] However, Tleoubaev mentioned that the thermal conductivity up to 20 W/mK can also be measured with lower accuracy.[6]

Therefore, this paper presents an apparatus to measure thermal conductivity up to 25 W/mK with a reasonable uncertainty based on the use of heat flux sensors. The designs of the heating system, the heat sink, the measuring system, and the vacuum chamber are presented in detail. The measurement procedures and the uncertainty are also given and discussed.

[a)]Author to whom correspondence should be addressed: 13b901004@hit.edu.cn

II. MEASUREMENT PRINCIPLE AND SIMULATION

The steady-state method for calculating thermal conductivity is based on Fourier's Law, which recommends a unidirectional and uniform heat flow across the sample between the hot plate and the cold plate with a stable temperature gradient. In general, Fourier's Law gives the relationship as

$$q = \lambda \frac{T_H - T_C}{\delta}, \tag{1}$$

where q is the heat flow across the specimen per unit area (W/m^2), T_H is the temperature of the sample surface in contact with the hot plate while T_C represents the sample surface temperature in touch with the cold plate (K), δ is the thickness of the sample (m), and λ is the thermal conductivity of the specimen (W/mK), which is related to the mean temperature $T_m = (T_H + T_C)/2$. Therefore, the thermal conductivity of the specimen is expressed as

$$\lambda = \frac{q \cdot \delta}{T_H - T_C}. \tag{2}$$

Temperature gradient inside the specimen, no less than three measurement points, needs to be directly measured by thermocouples placed in the holes drilled in the center of the specimen. Through the temperature gradient, T_H and T_C can be calculated by using the least-squares method or any other linear regression method. In addition, the thermal contact resistances between the surfaces of the specimen and the plates can be ignored. Therefore, the temperature difference between both sides of the specimen is reliable.

In the steady-state method, there are two ways to ensure the stability of one-dimension heat flow through the center of the specimen, using the sample itself or adding protective heaters. In this paper, a method for preventing heat flux loss by itself is adopted in the apparatus, and the specimen is surrounded by insulation cotton as well. The design of the cold plate is a passive configuration without temperature-controlled

and allows the temperature difference across the sample to freely float cooled through air convective heat transfer.[7] In order to verify the feasibility of this method, a numerical analysis is carried out by ANSYS to simulate the temperature gradient inside the specimen and the heat flux across it. The assumptions are made as follows: (a) two specimens are isotropic materials with thermal conductivity of 0.2 W/mK (material **A**) and 25 W/mK (material **B**), respectively; (b) a half of the specimen, with the dimension of 150 mm × 50 mm, is used during the analysis in order to observe the temperature difference and the heat flux through the center of the specimen; (c) the specimen and two plates are surrounded by the insulation cotton (50 mm in width) with a thermal conductivity of 0.2 W/mK. In the simulation, the temperature of 900 °C is loaded on one side of the sample while the surfaces of the insulation cotton and the cold plate which do not contact with the specimen are completely exposed to the conditions with the temperature of 25 °C and convective heat transfer coefficient of 5 W/m^{2}K. The model with the definite loads is shown in Fig. 1.

During the simulation, all lines are meshed by 1 mm. Since the radius of the heat flux meter is 8 mm, the radius of the central area which is regarded as the measuring area is assumed to be 10 mm. Figure 2(a) shows the temperature simulated result of material **A** of the entire model while Fig. 2(b) presents the temperature distribution inside the specimen. Similarly, when the specimen is material **B**, the numerical results are shown in Figs. 2(c) and 2(d). Therefore, the uniformity of heat flux through the center of the specimen can be checked by validating the temperature distribution.

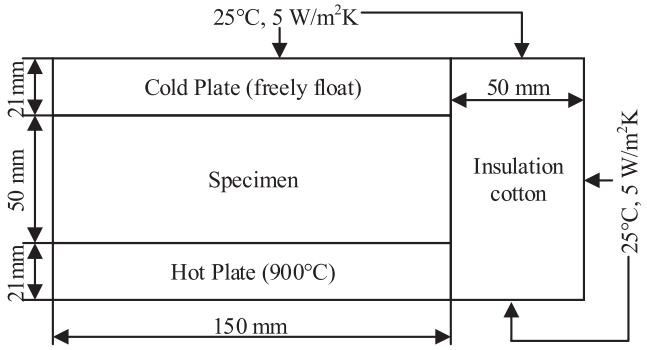

FIG. 1. The numerical model for analysis of this apparatus.

Additionally, in order to clarify whether this model can meet one-dimension heat flow conditions, the results of heat flux are also considered quantitatively. When the specimen is material **A**, the heat fluxes in and out the specimen are 2.22 × 10^3 W/m^2 and 2.20 × 10^3 W/m^2 through the center. The average heat flow across the specimen is 2.21 × 10^3 W/m^2. The heat fluxes across the material **B** are 5.26 × 10^3 W/m^2 and 4.73 × 10^3 W/m^2. The average heat flow is 5.00 × 10^3 W/m^2. It is clear that the system can meet one-dimension heat flux condition because the heat fluxes in and out the specimen are agreed with each other within about ±10%.[8]

Therefore, it is illustrated that this method is feasible to measure thermal conductivity of a material under 25 W/mK by heat dissipation freely of the specimen, especially in a vacuum environment where the convective heat transfer has little effect on the specimen.

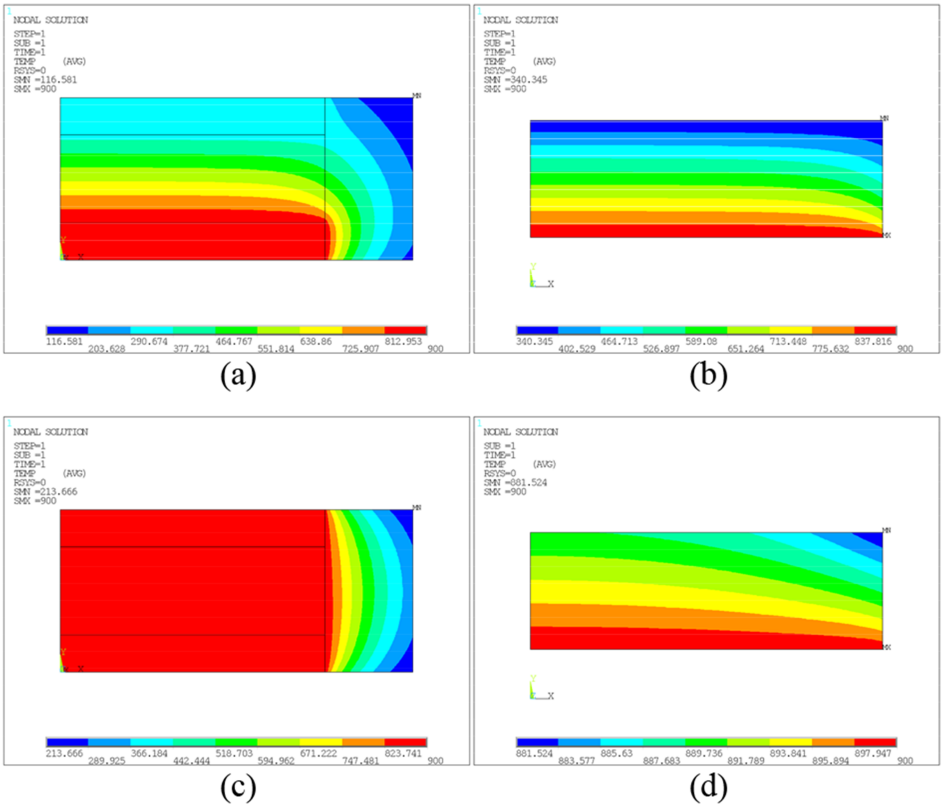

FIG. 2. (a) The numerical results for the model temperature distribution with material **A**. (b) The temperature distribution inside material **A**. (c) The numerical results for the model temperature distribution with material **B**. (d) The temperature distribution inside material **B**.

III. DESCRIPTION OF THE APPARATUS

The apparatus is designed for measuring the thermal conductivity up to 25 W/mK at a heating temperature range from 30 °C to 900 °C in a vacuum container of which the pressure can reach to 1 Pa.

The designed apparatus consists primarily of a heating system, heat sink, measurement system, vacuum system, and computer control system. The structure diagram of the apparatus is illustrated in Fig. 3. The apparatus uses two calibrated heat flux sensors to measure the heat flux across the specimen instead of calculating the input power of the measuring area. Furthermore, the cold plate is designed with no temperature-controlled system to create a natural temperature gradient inside the specimen. The software of this apparatus is written by Labview, using NI-DAQ to collect data from all the sensors. Besides, the vacuum system which controls the pressure individually is independent of the computer.

A. Heating system

The heating system consists of heating rods and a hot plate, and the temperature of the hot plate is controlled by the computer. The material of the plate is chosen by considering following factors: thermal conductivity (ensuring the uniformity of surface temperature), resistance to oxidation and high temperature performance (extending service life in high temperature testing), well performance of quick heating (heating the sample to the specified temperature rapidly), ease of machining, and convenience of maintenance.

The square hot plate (300 mm × 300 mm) is assembled by silicon carbide (SiC) with high thermal conductivity. The thickness is set to 21 mm to ensure temperature uniformity and enough mechanical properties. There are a number of advantages in using this material as a heater. First of all, SiC has a higher heating power per unit area than nichrome, so that it can reach the target temperature and achieve the steady state in a much shorter time. Besides, SiC has an average emittance of 0.81 with the wavelength region of 4-20 μm measured by the instrument designed by Wang[9] for auxiliary radiation heating. Moreover, SiC is easier to be machined than boron nitride (BN)[7] which has very high hardness. In addition, SiC has a proper thermal conductivity to reach the temperature uniformity. Therefore, the hot plate and heating rods of this apparatus are both made of SiC.

The plate is machined to fourteen semicircular grooves with the diameter of 7 mm evenly distributed on one side which is contacted with heating rods closely, as shown in Fig. 4. It is necessary to keep the temperature of the hot plate contacted with the specimen stable and uniform. The resistances of the heating rods are roughly the same to improve the heating efficiency and temperature uniformity. The central area of the plate, with the radius of 10 mm, is regarded as the measuring area. The hot plate is surrounded by insulation cotton (50 mm) to prevent the heat loss from the sides. In order to verify the temperature uniformity of the specimen surface, another numerical analysis is mentioned with the same conditions, and the simulated result is illustrated in Fig. 5. It is obvious that the

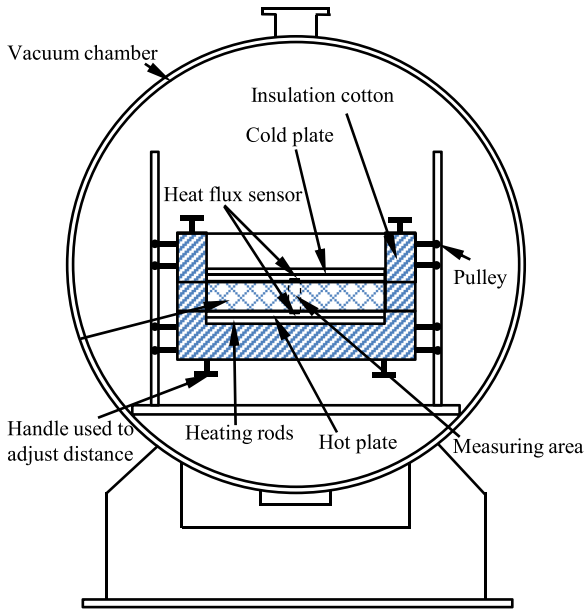

FIG. 3. The structure diagram of the apparatus.

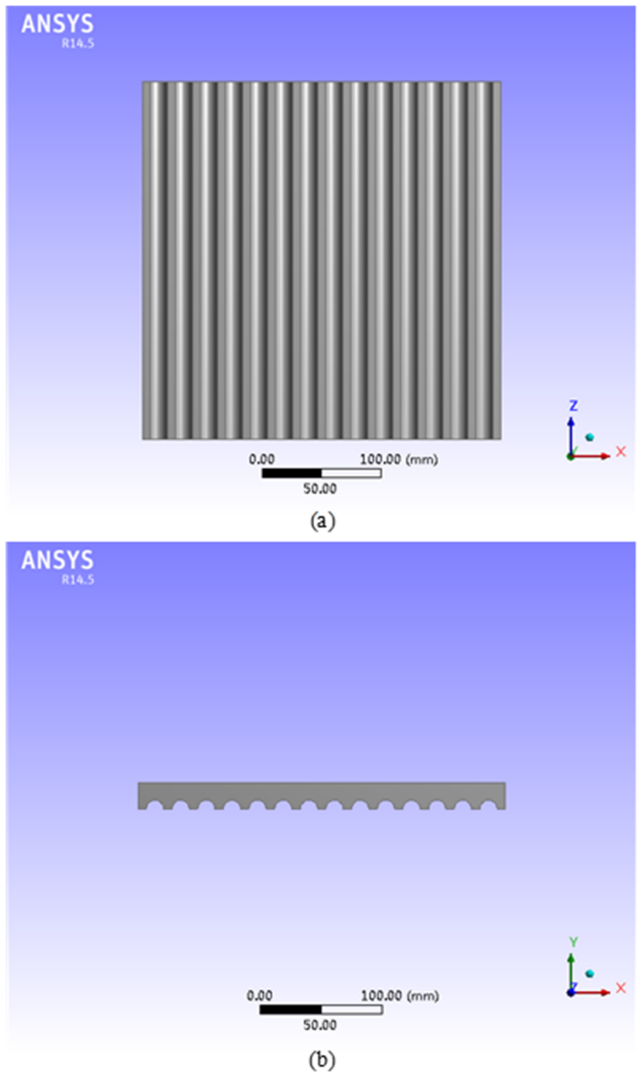

FIG. 4. The structure of the heating plate. (a) View from the bottom. (b) View from the front.

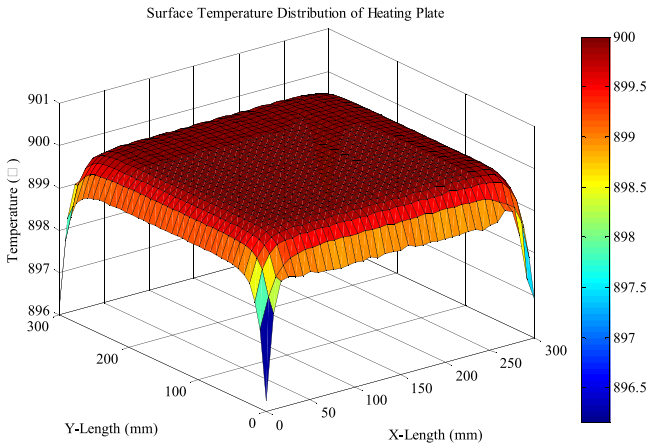

FIG. 5. Surface temperature distribution of the heating plate.

surface temperature of the hot plate can meet a good homogeneity, and the temperature difference of the hot plate through the center can be ignored.

Then, temperature-homogeneity experiments of the measuring area are performed with the setting temperature (T0) range from 100 °C to 900 °C for every 100 °C. Two thermal couples are implemented on the surface of the measuring area. T1 is placed in the center while T2 is placed at 10 cm away from the center. After reaching the steady state, the absolute values of maximal temperature differences calculated by T1 − T0 and T2 − T0 are illustrated in Fig. 6, respectively. It is obvious that the maximum temperature differences on the measuring area are less than 0.2 °C. Therefore, it is clear that the temperature on the measuring area of the hot plate can meet a good homogeneity.

B. Heat sink

The heat sink is designed to remove heat from the specimen. In the traditional steady-state device, the cold plate is maintained at a stable temperature with the closed-loop temperature-controlled. The temperature gradient depending on the temperature applied on the hot plate and the cold plate is a constant, which is not affected by the thermal conductivity of the specimen. Therefore, the precision of thermal conductivity totally depends on the accuracy of heat flux measurement.

In this apparatus, the cold plate which is regarded as the heat sink has the same structure and material as the hot plate. One side has a heat flux sensor embedded on the surface to measure the heat flux upon the specimen, and the other side is processed to fourteen semicircular grooves in order to enhance the contact area with the air. The feasibility of this design is simulated by finite element thermal modeling. The design creates a natural temperature gradient by allowing the heat across the specimen to freely float. Although the temperature gradient and the heat flux maybe different at repeated experiments, the result of thermal conductivity has small variations to the reference value.

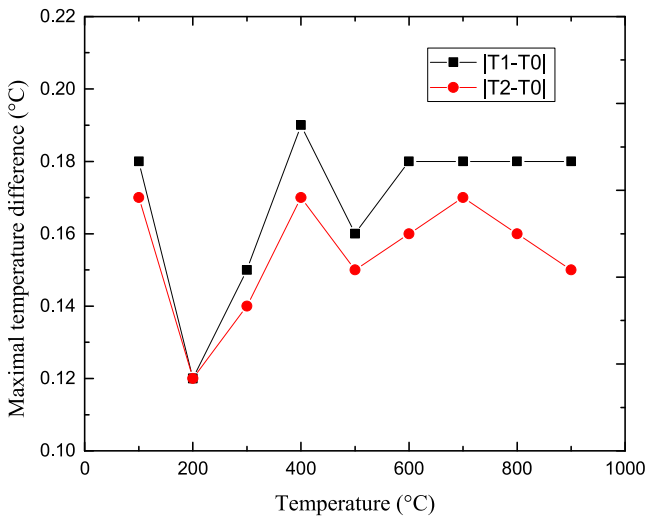

FIG. 6. Absolute value of maximal temperature differences of measuring area on the hot plate.

C. Measuring system

To calculate the thermal conductivity accurately, it is necessary to obtain the temperature gradient and heat flux through the specimen.

In the general method, the temperature gradient in the specimen is obtained by using the temperatures measured in the plates and is influenced significantly by thermal contact resistances between the specimen and the plates. For the material of high thermal conductivity, this effect cannot be ignored. Therefore, it is preferable to measure the temperature gradient directly inside the specimen. Several thermocouples, sheathed with stainless steel of 2 mm in diameter, are placed in the holes which are drilled in the specimen at different known distances from the surfaces. Then, the surface temperatures of both sides can be obtained by linear fitting of the temperature gradient. It is an accurate way to measure the temperature difference between T_H and T_C.

In the previous simulation analysis, the heat flux across the specimen can be considered as one-dimension heat flow. The heat flux sensors are embedded in both plates' surface contacted with the specimen. The heat flux across the specimen can be calculated by

$$q_s = \frac{q_H + q_C}{2}, \tag{3}$$

where q_H is the heat flux measured by the sensor embedded in the hot plate while q_C is obtained by the sensor assembled in the cold plate.

The heat flux sensor (HT-50) is manufactured by International Thermal Instrument Company. It is a flat plate transducer used to measure heat flow correctly by placing upon the surface or installing inside the plate with no loss of accuracy. The transducer is 15.9 mm in diameter and 3.5 mm in thickness. When the heat flow across the sensor, a direct current signal is created by a miniature, high temperature thermopile which is based on the small temperature difference between both surfaces of the sensor. Since the apparatus has a large temperature range, it is essential to calibrate the sensors at 30 °C and 100 °C–900 °C for every 100 °C using the standard of ASTM C-518.[10] Therefore, the sensitivity C (W m^{-2} μV^{-1}) of each heat flux sensor is given as a function of temperature

[Eqs. (4) and (5)],

$$C_1(T_1) = 2.82 \times 10^{-3} T_1 + 48.25, \quad (4)$$

$$C_2(T_2) = 2.59 \times 10^{-3} T_2 + 48.93. \quad (5)$$

Then, the heat flux across the specimen can be calculated by Eq. (6) in which $C_1(T_1)$ and $C_2(T_2)$ vary with temperature and E_1 and E_2 are regarded as the output voltage of heat flux sensors,

$$q = \frac{C_1(T_1) \cdot E_1 + C_2(T_2) \cdot E_2}{2}. \quad (6)$$

D. Vacuum system

The vacuum container with the cylinder of 1250 mm in diameter and 1500 mm in length is constructed with stainless steel. Hinged doors are designed on both sides of the container, which have the interlayer of water cooling in order to maintain the surface temperature of the vacuum container under 50 °C. The Roots vacuum pump unit contains a Roots pump as the main pump and a mechanical pump as the backing pump. In the process of vacuuming, the mechanical pump is used to reduce the pressure in the vessel to 1 kPa, then the Roots pump begins to work to make the pressure in the vessel reach the target vacuum degree. The vacuum system is controlled independently by the operating platform on the side of the container.

IV. EXPERIMENTAL RESULTS

To verify the accuracy and reliability of the new apparatus, we tested several materials of which thermal conductivities were known from other methods or references. Specimens of a heat insulation tile and 304L stainless steel were tested in different temperatures, respectively, while specimens made of *n*-docosane and erythritol were measured only at their solid state.

All the specimens had the dimension of 300 mm × 300 mm × 50 mm in the atmospheric pressure. For both specimens of the heat insulation tile and the 304L stainless steel, the samples were heated in the temperature range from 100 °C to 900 °C and measured for every 100 °C, and the experimental results are shown in Fig. 7. It is obvious that the tendency of thermal conductivity measured by this apparatus matched with the measurement results by Hotdisk or published data in the literature.

For phase change materials those would be researched in the future, the thermal conductivities of the *n*-docosane specimen and erythritol specimen were measured. Table I depicts the comparison of the experimental results by the apparatus designed in this paper and the testing results of Hotdisk. The transformation points of *n*-docosane and erythritol measured by differential scanning calorimetry are 42.3 °C and 119.0 °C, respectively. To the published values, the thermal conductivity of *n*-docosane ranges from 0.205 to 0.304 W/mK at room temperature.[12–14] For the material of erythritol, the value of thermal conductivity is 0.733 W/mK at room temperature[15,16] and reduces to 0.31 W/mK nearby the phase transformation point,[17] so that the thermal conductivity of erythritol decreases with increasing temperature at the solid state. Therefore, the reliability of the device designed in this paper is verified based on the analysis above.

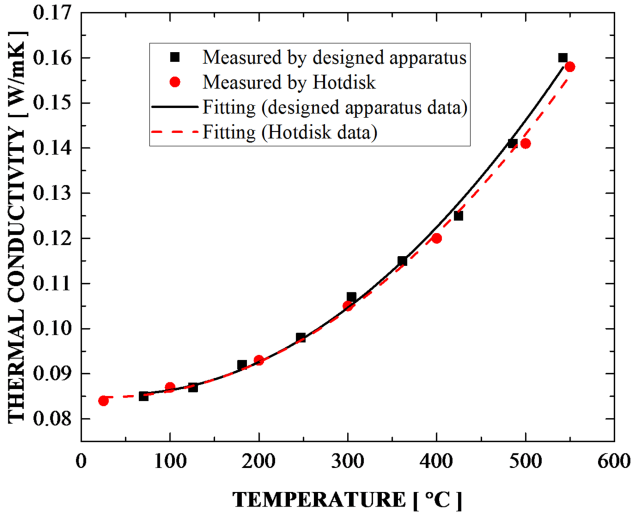

(a)

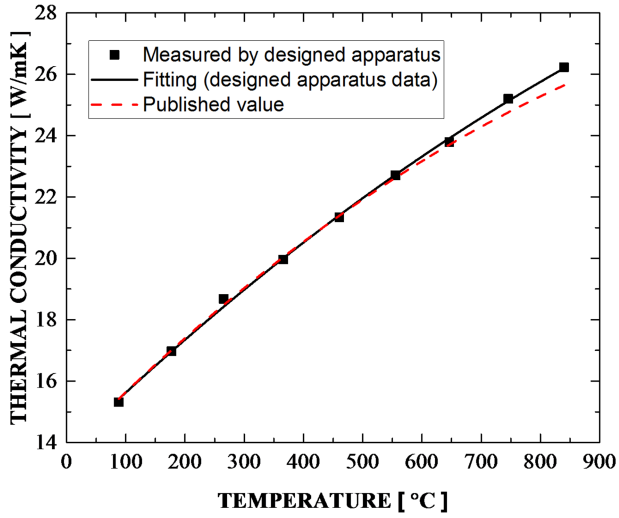

(b)

FIG. 7. Thermal conductivity of (a) the heat insulation tile and (b) 304L stainless steel.[11]

TABLE I. The comparison of the experimental results from designed apparatus and the testing results of Hotdisk.

Material	T_m (°C)	T_H (°C)	T_C (°C)	Thermal conductivity measured from designed apparatus Hotdisk (W/mK)	Thermal conductivity measured of
n-docosane	34.5	39.1	29.9	0.280	0.275
Erythritol	80.7	93.5	67.9	0.546	0.534

V. UNCERTAINTY ASSESSMENT

Before evaluating the uncertainty of thermal conductivity of the heat insulation tile and 304L stainless steel at different temperatures, several uncertainty sources need to be

considered including thermocouple calibration, thickness with thermal expansion, and heat flux sensor calibration.

A. Uncertainty of thermocouple calibration

The temperatures are measured by type K thermocouples. All the thermocouples have been carefully calibrated at fixed-point temperatures using a standard thermocouple (type S thermocouple of first-class standard). During the calibration, the sources of uncertainties are considered below.

First, the uncertainty of the standard thermocouple is taken into consideration. The upper limit of the recommended uncertainty of S type thermocouple is 0.6 °C or 0.1% of the measurement value (k = 2), which is greater. In other words, the uncertainty of the standard thermocouple is 0.6 °C (k = 2) when the temperature is under 600 °C while the uncertainty 0.1% (k = 2) is taken into account when the temperature is above 600 °C.

Second, the uncertainty of electromotive force (emf) measurement depends on the accuracy of the digital voltmeter. Based on the device specification, the digital voltmeter error can be calculated.

In addition, there are some other sources of uncertainty. Parasitic emf in the circuit is less than ±0.4 μV. Through PID control, the temperature fluctuation of the furnace and the reference temperature difference is less than ±0.05 °C, respectively. All these factors subject to the normal distribution at 95% confidence level.

Based on the analysis above, the standard uncertainty of the thermocouple calibration can be estimated, which is presented in Table II. The uncertainty of thermocouple calibration (u_{t-cal}) components includes the uncertainty of the standard thermocouple (u_S), the emf measurement uncertainties of the standard thermocouple and the type K thermocouple (u_{Semf} and u_{Kemf}), the uncertainties of the parasitic emf (u_{Sp-emf} and u_{Kp-emf}), the uncertainty of the temperature fluctuation (u_f), and the uncertainty of the reference temperature (u_{ref}). Besides, the differential thermal emf is taken into consideration. The result shows that the uncertainty of the type K thermocouple used in this apparatus is lower than the standard uncertainty of the type K thermocouple [2.2 °C or 0.75% of the measurement value (k = 2), which is greater].

In addition, T_H and T_C are obtained by linear fitting of the temperature gradient with calibrated thermocouples inside the specimen in this apparatus. Since ΔT and T_m are calculated by T_H and T_C, the combined uncertainties ($u_{\Delta T}$ and u_{Tm}) are obtained by

$$u_{\Delta T} = u_{Tm} = \sqrt{2 \times u_{t-cal}^2}. \tag{7}$$

Therefore, the standard uncertainty of temperature is depicted in Table III.

B. Uncertainty of thickness measurement

The thickness of the specimen and the locations of the thermocouples are measured by the vernier caliper with a scale interval of 0.02 mm, so that its quantization error is 0.01 mm. The error subjects to the uniform distribution. The standard uncertainty is expressed as

$$u_{\delta-vc} = \frac{1 \times 10^{-5}}{\sqrt{3}} = 5.80 \times 10^{-6}\ \text{m}. \tag{8}$$

The thermal expansion of the specimen is calculated by $\alpha(T - T_0)$, where α is the coefficient of thermal expansion which can be measured by DIL 402C, T is the temperature of the specimen, and T_0 is the reference temperature (25 °C) at which the thickness of the specimen is measured. Therefore, the uncertainty of the expansion can be calculated as

$$u_{\delta-ex} = \frac{\alpha(T - 25)\delta_0}{\sqrt{3}}, \tag{9}$$

where δ_0 refers to the original thickness measured before experiment. Besides, the standard uncertainty of DIL402C is expressed as

$$u_{DIL} = \frac{1 \times 10^{-8}}{\sqrt{3}} = 0.58 \times 10^{-8}\ \text{m}. \tag{10}$$

TABLE III. The standard uncertainty of temperature measurement.

T (°C)	u_{t-cal} (°C)	$u_{\Delta T}$ (°C)	u_{Tm} (°C)
100	0.064	0.091	0.091
200	0.074	0.104	0.104
300	0.076	0.107	0.107
400	0.078	0.110	0.110
500	0.079	0.112	0.112
600	0.082	0.116	0.116
700	0.097	0.139	0.139
800	0.114	0.161	0.161
900	0.134	0.189	0.189

TABLE II. The standard uncertainty of thermocouple calibration.

T (°C)	u_S (μV)	u_{Semf} (μV)	u_{Sp-emf} (μV)	u_{Kemf} (μV)	u_{Kp-emf} (μV)	u_f (μV)	u_{ref} (μV)	u_{t-cal} (μV)	u_{t-cal} (°C)
100	2.202	0.166	0.200	0.282	0.200	1.034	0.986	2.660	0.064
200	2.538	0.191	0.200	0.363	0.200	0.999	0.986	2.943	0.074
300	2.739	0.216	0.200	0.444	0.200	1.036	0.986	3.142	0.076
400	2.871	0.241	0.200	0.528	0.200	1.056	0.986	3.278	0.078
500	2.970	0.266	0.200	0.613	0.200	1.066	0.986	3.385	0.079
600	3.063	0.291	0.200	0.698	0.200	1.063	0.986	3.484	0.082
700	3.686	0.316	0.200	0.783	0.200	1.048	0.986	4.055	0.097
800	4.348	0.341	0.200	0.866	0.200	1.025	0.986	4.677	0.114
900	5.045	0.366	0.200	0.947	0.200	1.000	0.986	5.341	0.134

TABLE IV. The standard uncertainty of heat flux sensor calibration.

T (°C)	$\partial q_c/\partial\lambda_{9606}$ (°C/m)	$u_{\lambda 9606}$ (W/m °C)	$\partial q_c/\partial\delta_{9606}$ (W/m^3)	$u_{\delta 9606}$ (m)	$\partial q_c/\partial\Delta T$ (W/m^2 °C)	$u_{\Delta T}$ (°C)	u_{qc} (W/m^2)	u_{qc}/q_c (%)
100	787.402	0.064	-2.268×10^5	4.365×10^{-5}	289.764	0.090	57.545	1.986
200	787.402	0.060	-2.106×10^5	9.403×10^{-5}	270.866	0.104	58.212	2.149
300	787.402	0.056	-1.970×10^5	1.219×10^{-4}	254.331	0.107	57.097	2.245
400	787.402	0.054	-1.895×10^5	1.504×10^{-4}	245.669	0.110	57.884	2.356
500	787.402	0.052	-1.815×10^5	1.805×10^{-4}	236.220	0.112	58.741	2.487
600	787.402	0.051	-1.771×10^5	2.113×10^{-4}	231.496	0.116	61.056	2.638
700	787.402	0.050	-1.715×10^5	2.464×10^{-4}	225.197	0.137	65.253	2.898
800	787.402	0.049	-1.676×10^5	2.853×10^{-4}	221.260	0.161	70.922	3.205
900	787.402	0.047	-1.626×10^5	4.249×10^{-4}	215.748	0.189	76.464	3.544

Therefore, the standard uncertainty of thickness measurement can be estimated.

C. Uncertainty of heat flux sensor calibration

The uncertainty of heat flux relies on the uncertainty of the heat flux sensor adopted in this apparatus. Both sensors should be calibrated using the standard of ASTM C-518, in which Pyroceram 9606 is regarded as a standard material. The calibration formula is as follows:

$$q_c = \lambda_{9606}\cdot\Delta T/\delta_{9606}, \tag{11}$$

where $\lambda_{9606}(T_m)$ refers to the thermal conductivity of Pyroceram 9606, which is measured from 100 °C to 900 °C for every 100 °C. ΔT refers to the temperature difference between two surfaces of the standard specimen, which is 10 °C. δ_{9606} is the thickness of Pyroceram 9606, which refers to 12.70 mm. Therefore, the uncertainty of the heat flux sensor comes from the combined uncertainty of these factors.

Based on the calibration, the uncertainty of the heat flux sensor includes the uncertainty of the thermal conductivity measurement of Pyroceram 9606, the uncertainty of the thickness of Pyroceram 9606, and the uncertainty of temperature difference between two surfaces of this specimen. Table IV depicts the quantization parameters for the standard uncertainty of the heat flux meter in detail.

The measurement accuracy of Pyroceram 9606 thermal conductivity is ±3%, and the standard uncertainty heat subjects to the uniform distribution. Besides, the uncertainty of the thickness and temperature difference is analyzed above. Therefore, the standard uncertainty of flux measurement can be calculated by using the following formula:

$$u_{qc} = \sqrt{\left(\frac{\partial q_c}{\partial\lambda_{9606}}\right)^2 u^2_{\lambda 9606} + \left(\frac{\partial q_c}{\partial\delta_{9606}}\right)^2 u^2_{\delta 9606} + \left(\frac{\partial q_c}{\partial\Delta T}\right)^2 u^2_{\Delta T}}. \tag{12}$$

D. Uncertainty of the measurement of thermal conductivity

The measurement uncertainties of the designed apparatus are associated with the heat flow across the specimen, the temperature difference between the surfaces of the specimen, the thickness of the specimen, and the average temperature estimation of the sample. The combined standard uncertainty of the thermal conductivity measurement is derived from the combined variance of the error sources mentioned above by the following formula:

$$u_c = \sqrt{\sum_{i=1}^{n} c_i^2 (u_{xi})^2 + 2\sum_{1\le i<j}^{n} c_i c_j \rho_{ij} u_{xi} u_{xj}}, \tag{13}$$

where $c_i = \partial f/\partial x_i$ refers to the sensitivity coefficient; $u(x_i)$ refers to the standard uncertainty of the input parameter; ρ_{ij} is the correlation coefficient of any two direct measurement values. It is illustrated that all the input parameters are assumed to be uncorrelated in the mathematical model shown in Eq. (1).

TABLE V. Uncertainty budget of thermal conductivity measurements for 304L stain steel.

T_m (°C)	88.2	177.5	265.4	365.7	460.8	555.6	646.3	745.8	839.9
λ (W/m °C)	15.3	17.0	18.6	20.0	21.3	22.7	23.8	25.2	26.2
$\partial\lambda/\partial q$ (m/°C)	1.09×10^{-2}	8.70×10^{-3}	7.94×10^{-3}	7.25×10^{-3}	6.25×10^{-3}	5.38×10^{-3}	4.50×10^{-3}	3.79×10^{-3}	3.03×10^{-3}
$(u_q/q)^2$	3.94×10^{-4}	4.62×10^{-4}	5.04×10^{-4}	5.55×10^{-4}	6.18×10^{-4}	6.96×10^{-4}	8.40×10^{-4}	1.03×10^{-3}	1.26×10^{-3}
Relative weight of q	50.16%	58.29%	62.94%	67.52%	73.70%	78.48%	80.58%	82.50%	85.06%
$\partial\lambda/\partial\delta$ (W/m^2 °C)	3.06×10^2	3.39×10^2	3.72×10^2	3.99×10^2	4.27×10^2	4.54×10^2	4.76×10^2	5.04×10^2	5.24×10^2
$(u_\delta/\delta)^2$	4.50×10^{-7}	2.65×10^{-6}	6.79×10^{-6}	1.40×10^{-5}	2.36×10^{-5}	3.59×10^{-5}	5.05×10^{-5}	6.94×10^{-5}	9.03×10^{-5}
Relative weight of δ	0.06%	0.33%	0.85%	1.70%	2.81%	4.05%	4.84%	5.56%	6.10%
$\partial\lambda/\partial\Delta T$ (W/m °C^2)	−3.33	−2.95	−2.95	−2.89	−2.67	−2.44	−2.14	−1.91	−1.59
$(u_{\Delta T}/\Delta T)^2$	3.91×10^{-4}	3.28×10^{-4}	2.90×10^{-4}	2.53×10^{-4}	1.97×10^{-4}	1.55×10^{-4}	1.52×10^{-4}	1.49×10^{-4}	1.31×10^{-4}
Relative weight of ΔT	49.78%	41.38%	36.21%	30.78%	23.49%	17.47%	14.58%	11.94%	8.84%
u_{c-304L}(W/m·°C)	0.43	0.48	0.53	0.57	0.62	0.68	0.77	0.89	1.01
u_{c-304L}	2.80%	2.82%	2.83%	2.87%	2.90%	2.98%	3.23%	3.53%	3.84%

TABLE VI. Uncertainty budget of thermal conductivity measurements for the heat insulation tile.

T_m (°C)	70.3	125.8	181.1	247.1	304.2	361.6	424.6	485.8	542.2
λ (W/m °C)	0.085	0.087	0.091	0.097	0.105	0.113	0.122	0.137	0.155
$\partial\lambda/\partial q$ (m/°C)	8.74×10^{-4}	3.41×10^{-4}	2.12×10^{-4}	1.64×10^{-4}	1.28×10^{-4}	1.06×10^{-4}	9.11×10^{-5}	7.98×10^{-5}	7.01×10^{-5}
$(u_q/q)^2$	3.94×10^{-4}	4.62×10^{-4}	5.04×10^{-4}	5.55×10^{-4}	6.18×10^{-4}	6.96×10^{-4}	8.40×10^{-4}	1.03×10^{-3}	1.26×10^{-3}
Relative weight of q	98.87%	99.43%	99.19%	98.63%	98.05%	97.46%	96.98%	96.70%	96.55%
$\partial\lambda/\partial\delta$ (W/m^2 °C)	1.71	1.75	1.84	1.96	2.13	2.30	2.50	2.81	3.19
$(u_\delta/\delta)^2$	2.87×10^{-7}	1.44×10^{-6}	3.56×10^{-6}	7.40×10^{-6}	1.21×10^{-5}	1.80×10^{-5}	2.60×10^{-5}	3.50×10^{-5}	4.48×10^{-5}
Relative weight of δ	0.07%	0.31%	0.70%	1.32%	1.92%	2.52%	3.00%	3.28%	3.43%
$\partial\lambda/\partial\Delta T$ (W/m °C^2)	-1.49×10^{-3}	-5.96×10^{-4}	-3.89×10^{-4}	-3.22×10^{-4}	-2.74×10^{-4}	-2.43×10^{-4}	-2.28×10^{-4}	-2.25×10^{-4}	-2.24×10^{-4}
$(u_{\Delta T}/\Delta T)^2$	2.53×10^{-6}	5.03×10^{-7}	2.06×10^{-7}	1.30×10^{-7}	8.29×10^{-8}	5.93×10^{-8}	6.18×10^{-8}	6.61×10^{-8}	7.02×10^{-8}
Relative weight of ΔT	0.64%	0.11%	0.04%	0.02%	0.01%	0.01%	0.01%	0.01%	0.01%
$\partial\lambda/\partial T_m$ (W/m °C^2)	1.46×10^{-5}	4.68×10^{-5}	7.89×10^{-5}	1.17×10^{-4}	1.50×10^{-4}	1.84×10^{-4}	2.20×10^{-4}	2.56×10^{-4}	2.88×10^{-4}
$(u_{\Delta T}/T_m)^2$	1.67×10^{-6}	6.85×10^{-7}	3.50×10^{-7}	1.97×10^{-7}	1.36×10^{-7}	1.03×10^{-7}	1.04×10^{-7}	1.10×10^{-7}	1.21×10^{-7}
Relative weight of T_m	0.42%	0.15%	0.07%	0.03%	0.02%	0.01%	0.01%	0.01%	0.01%
u_{c-tile} (W/m °C)	0.0017	0.0019	0.0021	0.0023	0.0027	0.0031	0.0037	0.0046	0.0058
u_{c-tile}	1.99%	2.15%	2.25%	2.37%	2.51%	2.67%	2.94%	3.26%	3.61%

For the specimen of 304L stainless steel, it can be assumed that the thermal conductivity varies linearly between T_H and T_C at each measurement because the maximum temperature difference is 17.3 °C. So this uncertainty factor is negligible. Table V gives the standard uncertainty of thermal conductivity measurement for 304L stainless steel and also depicts the variance for each factor as a function of temperature.

When the heating temperature is 100 °C, it is illustrated that the influence of heat flux and temperature difference is almost the same. If the heating temperature rises, the uncertainty of the heat flux measurement has the most influence.

For the specimen of the heat insulation tile, the thermal conductivity measured by this apparatus is regarded as the effective thermal conductivity at T_m. Furthermore, based on the fitting curve, the sensitivity coefficient of T_m can be estimated. Table VI gives the uncertainty budget of thermal conductivity measurement for the heat insulation tile with a function of temperature. It is illustrated that the heat flux is the most important uncertainty factor.

Therefore, the maximum relative expanded uncertainty (at 95% confident levels) for the thermal conductivity measurement is evaluated to be 7.68% for the medium conductivity material (304L stainless steel) and 7.22% for the low conductivity material (heat insulation tile).

VI. CONCLUSION

In this paper, an apparatus based on the steady state method has been designed and constructed with the heating temperature range from 30 °C to 900 °C to measure thermal conductivity up to 25 W/mK. The material and structure of the heating plate are different from the traditional method. Meanwhile, simulation of the heating plate ensures the temperature uniformity. Furthermore, experimental results are reliable compared with the data measured by the Hotdisk method or published in the literature. By analyzing the uncertainty of 304L stainless steel and heat insulation tile at different heating temperatures, it enables to see which parameters have the most influence on the thermal conductivity measurement depending on different temperatures and materials. Therefore, the parameter measured by this new apparatus is accurate and reliable.

ACKNOWLEDGMENTS

This work is supported by National Technical Basic Research Program of China (Grant No. JSZL2015603B002).

[1] W. Hemminger and R. Jugel, Int. J. Thermophys. **6**, 483 (1985).
[2] M. F. Li, H. Zhang, and Y. L. Ju, Rev. Sci. Instrum. **83**, 075106 (2012).
[3] V. Scoarnec, J. Hameury, and B. Hay, Int. J. Thermophys. **36**, 540 (2015).
[4] M. M. Terzic, N. D. Milosevic, N. M. Stepanic, and S. J. Petricevic, Therm. Sci. **20**, S321–S329 (2016).
[5] G. A. Longo, Int. J. Thermophys. **29**, 664 (2008).
[6] A. Tleoubaev and A. Brzezinski, *Thermal Conductivity 27: Thermal Expansion 15* (Destech Publications, 2005), Vol. 27, p. 502.
[7] B. J. Filla, Rev. Sci. Instrum. **68**, 2822 (1997).
[8] ASTM Standard Test Method E1225-13, Annual Book of ASTM Standards, Vol. 14.05, 2013.
[9] Z. W. Wang, J. M. Dai, X. W. He, C. L. Yang, and X. F. Cui, Proc. SPIE **7656**, 76563Q (2010).
[10] ASTM Standard Test Method C518–15, Annual Book of ASTM Standards, Vol. 04.06, 2015.
[11] R. S. Graves, T. G. Kollie, D. L. McElroy, and K. E. Gilchrist, Int. J. Thermophys. **12**, 409–415 (1991).
[12] M. Li and Z. S. Wu, J. Therm. Anal. Calorim. **111**, 77 (2013).
[13] Z. H. Rao, S. F. Wang, Y. L. Zhang, F. F. Peng, and S. H. Cai, Acta Phys. Sin.-Chin. Ed. **62**, 056601 (2013).
[14] A. Sari and A. Karaipekli, Appl. Therm. Eng. **27**, 1271 (2007).
[15] T. Oya, T. Nomura, M. Tsubota, N. Okinaka, and T. Akiyama, Appl. Therm. Eng. **61**, 825 (2013).
[16] I. Kholmanov, J. Kim, E. Ou, R. S. Ruoff, and L. Shi, ACS Nano **9**, 11699 (2015).
[17] H. K. Shin, K. Y. Rhee, and S. J. Park, Composites, Part B **96**, 350 (2016).